Journal of Advanced Ceramics
2014, 3(3): 230–239
DOI: 10.1007/s40145-014-0114-0

ISSN 2226-4108
CN 10-1154/TQ

Research Article

Evaluation of SiC–porcelain ceramics as the material for monolithic catalyst supports

Oleg SMORYGO[a,*], Alexander MARUKOVICH[a], Vitali MIKUTSKI[a], Vladislav SADYKOV[b]

[a]*Powder Metallurgy Institute*, *41*, *Platonov Str.*, *220005*, *Minsk*, *Belarus*
[b]*Boreskov Institute of Catalysis*, *5*, *Lavrentiev Ave.*, *630090*, *Novosibirsk*, *Russia*

Received: April 14, 2014; Revised: June 17, 2014; Accepted: June 20, 2014

Abstract: Mechanical and thermal properties of SiC–porcelain ceramics were studied in the wide SiC content range of 0–95%. Microstructure evolution, shrinkage at sintering, porosity, mechanical strength, elastic modulus, coefficient of thermal expansion (CTE) and thermal conductivity were studied depending on SiC content. The optimal sintering temperature was 1200 ℃, and the maximum mechanical strength corresponded to SiC content of 90%. Parametric evaluation of the ceramic thermal shock resistance revealed its great potential for thermal cycling applications. It was demonstrated that the open-cell foam catalyst supports can be manufactured from SiC–porcelain ceramics by the polyurethane foam replication process.

Keywords: SiC; porcelain; mechanical properties; thermal properties; foam

1 Introduction

Efficiency of catalytic process with strong heat flux (e.g., hydrocarbon steam reforming) is strongly dependent on the catalyst thermal conductivity. Catalysts supported on the metal alloy monolithic supports ensure effective heat transfer in reactors thus providing a uniform temperature distribution (both axial and radial), and this affects overall catalyst performance [1–3]. Low robustness of metallic catalyst supports due to corrosive degradation in the reaction media (600–900 ℃, water vapor, decomposition products of hydrocarbon, aggressive admixtures) limits their practical application [1,4]. This problem does not arise when the catalyst supports are made from various oxide ceramics exhibiting excellent corrosive resistance [5–7]. Conventional oxide ceramics, however, have low thermal conductivity which can be the cause of strong temperature gradients within catalytic reactor, and local hot zones can appear resulting in the catalyst sintering and its fast deactivation [8]. The use of the silicon carbide catalyst supports in the hydrocarbon steam reforming and other strongly endothermic or exothermic process [9] looks promising taking into account their attractive combination of high thermal conductivity and excellent corrosive resistance. The data in Ref. [10] demonstrated that the substitution of the alumina foam catalyst supports by the silicon carbide ones results in the increase of the cobalt based catalyst selectivity from 54% to 80% due to more uniform temperature distribution in the reactor.

Extensive application of SiC catalyst supports is restrained by the considerable manufacturing cost resulting from high sintering temperature of above 2100 ℃ [11]. Ceramic materials with high SiC content (up to 90%–95%) and high mechanical strength

* Corresponding author.
E-mail: olegsmorygo@yahoo.com

(450–500 MPa) as well as SiC foam catalyst supports can be synthesized via liquid phase sintering with sintering aids like Al_2O_3–Y_2O_3 [12,13]. This process is often classified as "low temperature sintering", but actually the sintering occurs at rather high temperatures of 1700–1800 ℃. Besides, the process implies protective sintering atmospheres in order to prevent SiC oxidation, which also contributes to the product manufacturing cost. That is why many efforts were undertaken during the last decade to develop compositions ensuring SiC based ceramics at much lower sintering temperatures. It was found that ceramic materials with high SiC content and reasonable mechanical properties can be synthesized by sintering in air with alkali or alkali-earth silicate sintering aids at temperatures as low as 1100–1200 ℃ [14–19]. Various sintering aids containing alkali oxides were successfully applied in these researches: porcelain and its polishing residues, bentonite, and art glass. Potentially, if a reasonable combination of mechanical and thermal properties can be attained, this type of ceramics can have a great commercial potential as the material for monolithic catalyst supports: its low manufacturing cost is predetermined by cheap initial materials and low sintering temperature without special protective atmosphere. However, no study performed complex analysis of mechanical and thermal properties of this type of ceramics before, and no study estimated this type of ceramics as the material for monolithic catalyst supports. Besides, the referred papers presented experimental data on different and rather narrow SiC content ranges, and hence the authors did not report on the evolution of microstructure and properties in the whole SiC content range.

In this paper, we studied sintering regimes, microstructure evolution, and mechanical and thermal properties of SiC–porcelain ceramics in the wide SiC content range of 0–95%. Complex analysis of properties that influence the performance in thermal cycling applications was performed, and SiC–porcelain ceramics' potential as the catalyst support material was analyzed via parametric evaluation. It was demonstrated that open-cell ceramic foam catalyst supports can be manufactured from this type of ceramics by the polyurethane foam replication process.

2 Experimental procedures

Industrial porcelain slip and technical-grade silicon carbide powder (d_{50} = 10.5 μm, purity > 98%) were used in this study. The slip was received from PJSC "Dobrush Porcelain Factory", Belarus; its chemical composition is given in Table 1. The compositions were prepared as follows. The porcelain slip was dried at 110 ℃ and then mixed with the silicon carbide powder in aqueous media using a high-velocity stirrer (250 rpm, 1 h). Then the mixture was dried at 110 ℃, and 10% polyvinyl alcohol (PVA) aqueous solution (10 wt%) was added. Ceramics and PVA solution were mixed in porcelain mortar, and after rubbing through the sieve with the opening size of 100 μm, experimental samples were prepared by uniaxial die pressing (100 MPa). SiC content in the mixture varied within 0–95 wt% (related to the porcelain's solid) in this study. Dimensions of the samples were dependent on the characterization procedure; the details will be given below. After drying at room temperature for 24 h and at 110 ℃ for 4 h, the samples were heated in an electric furnace to the sintering temperature (1100–1250 ℃, 10 ℃/min) and sintered in air atmosphere for 1 h.

Mechanical properties (three-point bending strength and elastic modulus) were studied using Tinius Olsen H150KU testing machine, and the sample dimensions were 55 mm × 10 mm × 5 mm. The same samples were used for measuring open porosity by hydrostatic weighing in ethanol. Scanning electron microscope (SEM) Mira, Tescan, with energy dispersive X-ray (EDX) analyzer INCA-350, Oxford Instruments, was used for the fracture surface and microstructure examinations. Prior to the microstructure examination, the samples were mounted with the epoxy resin, ground following usual metallographic routines and finally etched at room temperature in 5% HF aqueous solution for 30 s. Coefficient of thermal expansion (CTE) was measured in vacuum within the temperature range of 20–500 ℃ using Netzsch 402-E horizontal pushrod dilatometer; the samples with diameter of 7 mm and length of 25 mm were examined. Thermal conductivity coefficient was measured at room temperature under the steady-state thermal conditions using IT-2 thermal conductivity meter, RIAPP, Belarus;

Table 1 Chemical composition of porcelain and its loss of ignition (LOI) at 1200 ℃

Chemical composition (wt%)							LOI
Al_2O_3	SiO_2	K_2O	Na_2O	Fe_2O_3	CaO	TiO_2	(wt%)
25.07	70.59	2.04	0.90	0.52	0.46	0.42	7.1

the sample dimensions were 15 mm × 15 mm × 0.5 mm.

Open-cell foam catalyst supports were manufactured from SiC–porcelain composition with optimal combination of mechanical and thermal properties via the polyurethane foam replication route. Details of the process applied in this study are described in Ref. [20].

3 Results and discussion

3.1 Processes during the sintering

The sintering regimes of SiC–porcelain ceramics are pre-defined by interactions that occur at temperatures of above 1000 ℃; major interactions and the accompanying microstructure changes in this system were described before in Refs. [21–23]. In brief, SiC particles are protected by a thin vitreous silica film at normal conditions, which ensures excellent corrosive resistance of SiC ceramics in air. However, when temperature exceeds the melting point of the alkaline salts in porcelain, the silica film reacts with the molten salt, and it results in the formation of the alkaline silicate liquid. Thus, silica film is broken due to corrosion; oxygen diffuses easily to SiC and reacts with it. Silica and gaseous carbon oxides are the products of this reaction. If outward release of the gaseous products is hindered, they are entrapped by the silicate melt (liquid phase), and intensive generation of the secondary porosity occurs. The increase of sintering temperature favors accelerated corrosion of the protective layer, and it results in the increased final porosity and coarser pores. If the temperature is too high, the surface swelling and even formation of a highly-porous cellular structure in the sample's volume can be observed. Hence, optimization of sintering conditions for the studied compositions implies the compromise between maximum possible densification due to the liquid phase sintering, on one hand, and the absence of bubbling due to the gaseous product releasing, on the other hand. Different authors who studied SiC interaction with the alkali silicate melt sintering aids stated rather close optimal sintering temperatures; some non-principal deviations can be referred to differences in the sintering aid compositions and different targeted SiC content ranges in the ceramics. The reported sintering aids and corresponding optimal temperatures are as follows: Li_2O–Al_2O_3–SiO_2, 1150 ℃ [17]; bentonite, 1100 ℃ [14]; porcelain tile residues, 1200 ℃ [23]; porcelain, 1180 ℃ [22].

In order to determine preferable sintering temperature for the studied SiC–porcelain system, samples with SiC content of 85% were sintered in air for 1 h at temperatures ranging from 1100 ℃ to 1250 ℃. Dependence of the linear shrinkage on sintering temperature is demonstrated in Fig. 1. The shrinkage is not strongly dependent on temperature and just slightly decreased from 1.65% to 1.2% with the sintering temperature increase. SiC is the reactive filler towards porcelain, and hence the ceramic shrinkage is the resultant of the following phenomena: (I) densification due to the liquid phase formation; (II) formation of less dense phase due to SiC oxidation to SiO_2 during sintering (ρ = 3.21 g/cm^3 and ρ = 2.2 g/cm^3 for SiC and vitreous silica, respectively); (III) expansion due to the gas generation and consequent bubbling the liquid phase (resulting from SiC reaction with the alkali silicate melt). For the studied system, the driving forces of the volumetric expansion compensate the driving forces of the ceramic shrinkage: higher sintering temperatures result in more intensive SiC oxidation, and hence more intensive SiO_2 formation and gas generation. That is why obvious increase of the shrinkage with the sintering temperature increase is not observed. Furthermore, some shrinkage decrease is stated. Visible surface glass swelling and large bubbles at the sample surface are observed after sintering at 1250 ℃ (Fig. 2). Besides, coarse and isolated round pores are detected inside the samples, which is resulted evidently from the gas generation and its entrapment during the sintering. Samples sintered at 1200 ℃ retain their original shape without any change of the surface condition, and this sintering temperature is used in all further studies.

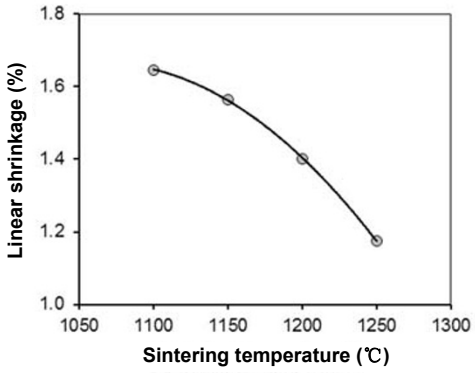

Fig. 1 Effect of sintering temperature on linear shrinkage (85% SiC).

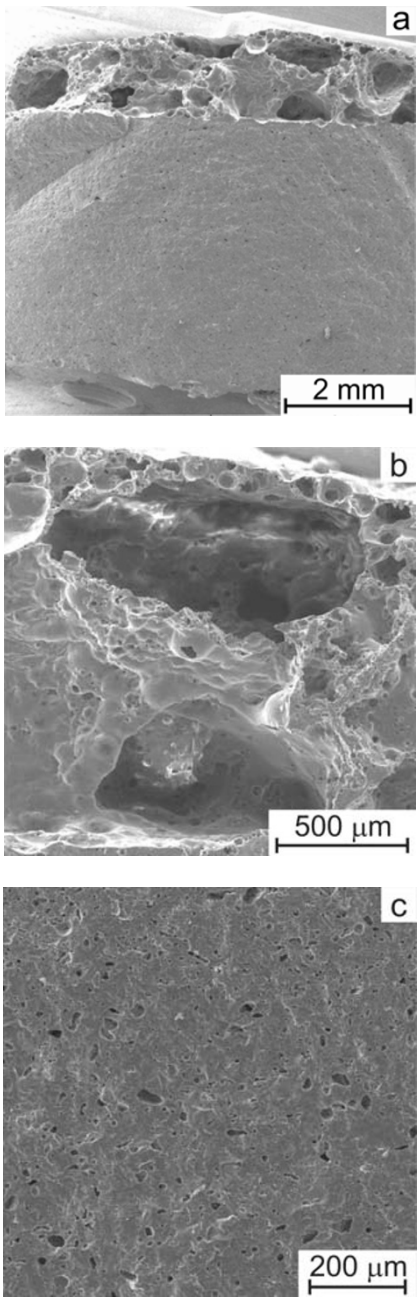

Fig. 2 SEM images of the SiC–porcelain sample with the surface glass swelling (85% SiC, 1250 ℃): (a) fracture surface; (b) bubbles on the top surface; (c) bulk microstructure.

Microstructures of the porcelain and SiC–porcelain ceramics sintered at 1200 ℃ are presented in Fig. 3. As it is expected, remarkable residual porosity with the pooled glass inclusions can be observed in the porcelain sample; regular sintering temperature of this porcelain is 1340–1360 ℃ according to the supplier. At low and medium SiC contents, both SiC grains and pooled glass inclusions are observed, and the intergrain phase has evidently higher residual porosity compared to pure porcelain. At the highest SiC content, SiC grains are bound by a highly porous glassy phase. Compositional and resultant microstructural differences among the different ceramics in this study affect their properties, which will be discussed in the following.

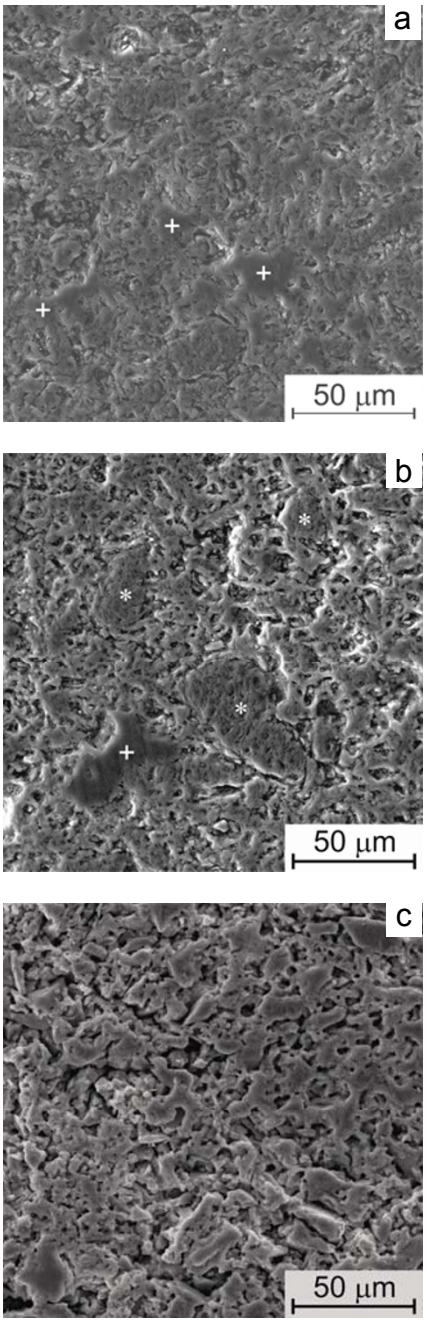

Fig. 3 SEM images of the microstructure of SiC–porcelain ceramics at different SiC contents: (a) porcelain; (b) 40% SiC; (c) 85% SiC. Pooled glass is marked with "+"; SiC grains are marked with " * ".

Figures 4, 5 and 6 enable to analyze the evolutions of ceramic shrinkage at sintering, apparent density and open porosity depending on SiC content, respectively. Linear shrinkage decreases from 6.8% to 0.8% with SiC content increase. At the same time, there is no strict correlating dependence for the sample apparent density that decreases from 2.27 g/cm^3 to 2.01 g/cm^3 only in the same SiC content range. Taking into account large difference among densities of the ceramic constituents (ρ=2.27 g/cm^3 and ρ=3.21 g/cm^3 for the studied porcelain and SiC, respectively), one can state that the expected density increase is compensated by the residual porosity increase. The comparative analysis of Figs. 5 and 6 reveals that the apparent density decrease by 11.5% is accompanied by the open porosity increase from 15% to 46%, which is equivalent to 1.5-fold relative density decrease. Gradual elimination of closed porosity that is not measurable by the applied method and simultaneous formation of open porosity at higher SiC contents are the most evident reasons of this mismatch.

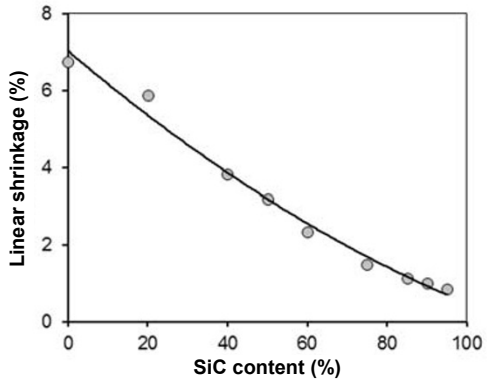

Fig. 4 Effect of SiC content on linear shrinkage at sintering.

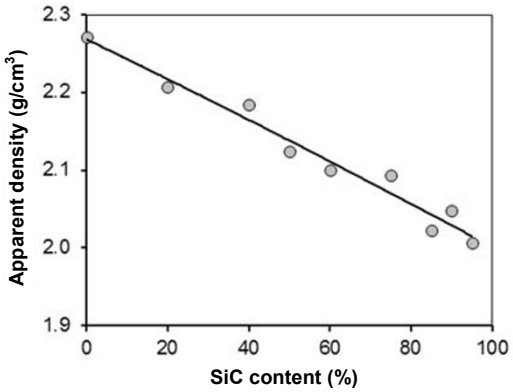

Fig. 5 Effect of SiC content on apparent density.

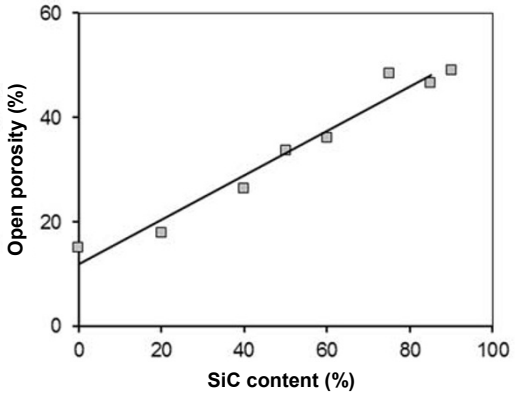

Fig. 6 Effect of SiC content on open porosity.

Formation of the predominantly open porosity is stated to favor faster SiC oxidation during the sintering in air. The effect of SiC content on SiC oxidation rate during the sintering can be understood from Figs. 7 and 8. The weight loss after sintering of compositions with the lowest SiC contents changes to the weight gain at its higher contents. In Fig. 7, the solid line is the measured weight change after sintering at 1200 ℃ for 1 h. This dependence results from two simultaneous phenomena: the porcelain weight loss of ignition (LOI) and the weight gain due to SiC oxidation. Contribution of the porcelain weight loss can be easily estimated from its portion in the initial mixture and the measured LOI is 7.1%; the dashed line in the graph corresponds to this dependence. Subtraction of the dashed line from the solid line gives the dashed-dot line demonstrating the weight gain due to SiC oxidation. Assuming that all the oxidized SiC is transformed to SiO_2, one can estimate the rate of the oxidized SiC in the ceramics depending on its composition (Fig. 8). Larger open porosity seems to be the only reason of the more intensive SiC oxidation: the open porosity favors easier oxygen supply to the non-protected SiC particle surfaces as well as much

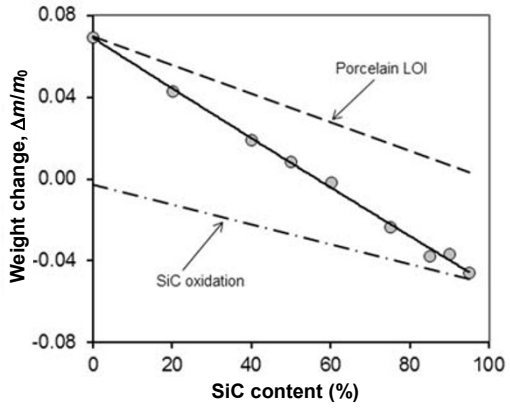

Fig. 7 Effect of SiC content on the ceramic weight change after sintering.

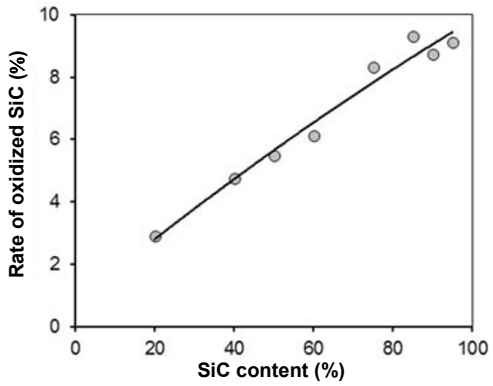

Fig. 8 Effect of SiC content on estimated rate of oxidized SiC.

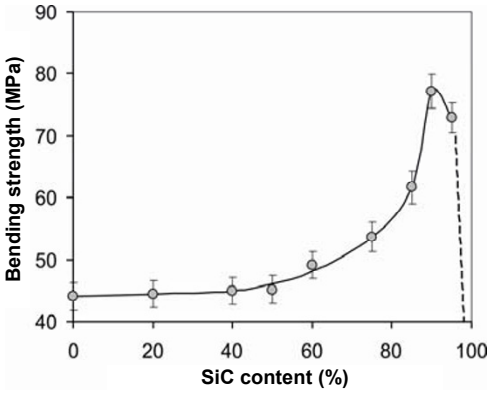

Fig. 9 Effect of SiC content on bending strength.

easier release of the gaseous SiC oxidation products. According to this estimation, up to 9% of total SiC amount oxidizes during the sintering. This fact must be taken into account when monolithic catalyst supports with high surface-to-volume ratio are manufactured. The surface-to-volume ratio of the bar-type samples used in this study is ~640 m^2/m^3. Specific surface area of the open-cell foam catalyst supports with typical 10–30 ppi cell size grades (this corresponds to the cell diameter range of ~2–6 mm) and open porosity of 0.85 is roughly equal to ~330–1000 m^2/m^3 [24]. This is very close to the same parameters of the experimental samples, and similar oxidation rate can be expected.

3.2 Mechanical properties

As it can be seen in Fig. 9, the bending strength is almost independent on SiC content until 60% of SiC (55–59 MPa). Further SiC content increase results in the fast strength increase that attains the maximum value at 90% of SiC (77 MPa). Hypothetic continuation of experimental curve is given as the dashed line in the graph. Thus, direct correlation between the ceramic residual porosity and its mechanical strength is not stated. Similar strength maxima are observed in the SiC–art glass system at 90% of SiC [18] and SiC–bentonite system at 90%–95% of SiC [14]. In Ref. [18], such maximum is referred to the best dispersion of the binding glass phase throughout the composite; at higher glass loadings it forms continuous phase with low toughness and significant pooling, which facilitates the crack initiation and propagation. Fracture surface images of different compositions synthesized in this research are demonstrated in Fig. 10. The fracture surface views are similar in porcelain and SiC–porcelain ceramics at low

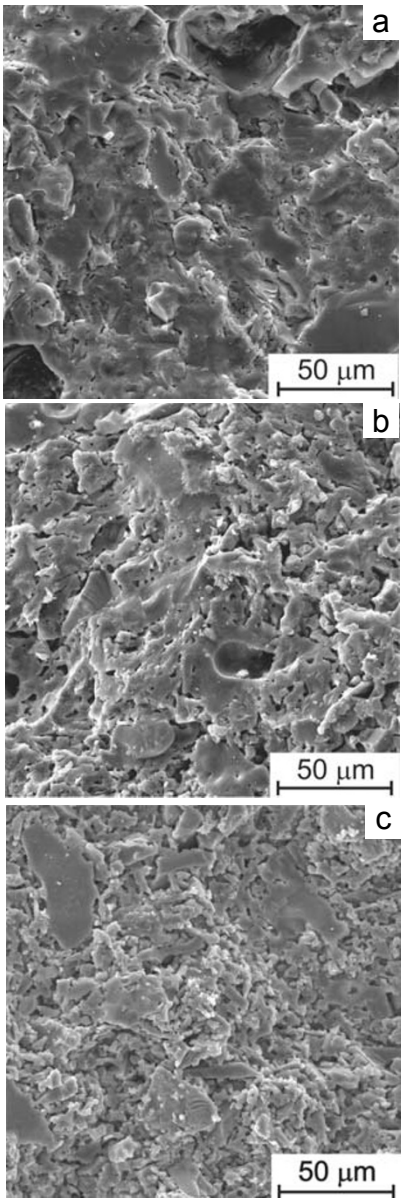

Fig. 10 SEM images of the SiC–porcelain ceramic fracture surfaces at different SiC contents: (a) porcelain; (b) 20% SiC; (c) 85% SiC.

and medium SiC contents, because the fracture runs through the porcelain phase in all cases. That is why SiC grains can not be differentiated in Figs. 10(a) and 10(b). The presence of SiC in the ceramics could be only detected indirectly due to much higher residual porosity generated because of SiC oxidation. At the highest SiC content, the fracture occurs predominantly along the SiC–porcelain interface, which presumably must be responsible for the sharp mechanical strength increase.

Thus, based on the mechanical strength and microstructure investigations, one can distinguish three characteristic SiC content areas with different fracture behaviors. At low and medium SiC contents (less than 50%–60%), the measured strength values are very close (i.e., the deviations are within the experimental error). In this content range, SiC grains are distributed loosely in the binding porcelain phase. That is why the crack runs through this phase, the crack path is linear, and the bending strength is controlled by this phase. Sharp strength increase with the SiC content increase from 60% to 90% can be explained by gradual microstructure changes. In this range, the space among SiC particles is still filled by the porcelain phase, but the crack path becomes tortuous, and deflection of the crack path becomes more and more significant since the packing density of strong SiC grains is increasing [25]. Further SiC content increase results in the strength decrease because the porcelain binding phase does not fill the intergranular space, and, according to the minimum solid area model for porous materials [26], mechanical strength of porous ceramics σ is related to its porosity ε by the equation $\sigma = \sigma_0 \exp(-b\varepsilon)$, where σ_0 is the strength of the corresponding fully dense material and b is a constant depending on the pore shape and alignment. Finally, the curve on Fig. 9 must tend to zero as far as SiC content approaches 100% since direct sintering of SiC is impossible at such low temperatures [27].

Similar but not so pronounced dependence is stated for elastic modulus (Fig. 11): it is initially invariable, but increases at the highest SiC contents. Unfortunately, exact location of the modulus maximum is not stated in this study; hypothetical continuation of the curve is given as the dashed line in the graph. It should be emphasized that the elastic modulus values are rather low in all the studied range due to high residual porosity (~9–11 GPa). It also should be noted that,

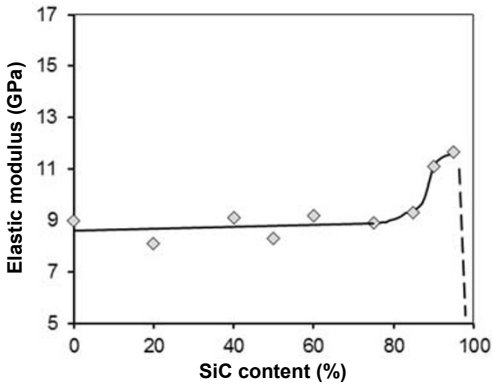

Fig. 11 Effect of SiC content on elastic modulus.

according to the additivity law [28], elastic modulus value is expected to increase smoothly with the SiC fraction increase in all the SiC content range that ensures continuous filling of the intergranular space between SiC grains with the porcelain phase (i.e., until 85%–90% of SiC). However, the expected increase of the modulus seems to be compensated by the increasing residual porosity. The increase of the modulus value in Fig. 11 at SiC content of 90%–95% presumably results from the tightest packing of SiC grains within the porcelain matrix. Further sharp drop of elastic modulus value to zero can be expected taking into account the minimum solid area model [26] and the fact that SiC grains cannot be sintered directly at 1200 ℃.

3.3 Thermal properties

Evolutions of the ceramic thermal properties (CTE and thermal conductivity) depending on SiC content are illustrated in Figs. 12 and 13. As it is expected, CTE gradually decreases and thermal conductivity increases with the SiC content increase; near-linear dependencies are observed in both cases in the studied range. Thermal conductivity coefficient is equal to ~10–12 W/(m·K) at the highest SiC contents, which is comparable by value of magnitude to the same parameter of stainless steels and nickel-chromium alloys. The measured thermal properties in combination with mechanical properties provide the necessary data to estimate thermal shock resistance of the synthesized ceramics. The strength controlled thermal fracture resistance of the engineering ceramics can be roughly estimated using statistical parameters $R = \sigma_f/(\alpha E)$ (high heat transfer) and $R' = \lambda\sigma_f/(\alpha E)$ (low heat transfer) [29], where λ is the thermal

conductivity coefficient; σ_f is the stress to failure; α is the CTE; and E is the elastic modulus. Dependencies calculated from experimental data are presented in Fig. 14; both R and R' values increase with the SiC content increase. Analysis of these experimental curves and the data on many usual engineering ceramics [29] reveals superior R and R' values of the studied SiC–porcelain ceramics with SiC content of 85%–90% compared to conventional cordierite, mullite and Y-PSZ. This makes the alkali silicate bound SiC ceramics a rather attractive object of detailed studies in the thermal cycling and thermal shock applications (e.g., as catalyst supports), because the production cost benefits can be expected due to comparatively low sintering temperature, simple sintering regimes and cheap raw materials. However, practical operating temperature range, durability and thermal shock behavior of this type of ceramics should be studied in more detail in further researches.

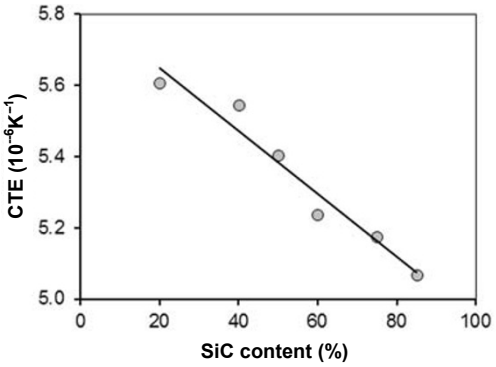

Fig. 12 Effect of SiC content on coefficient of thermal expansion.

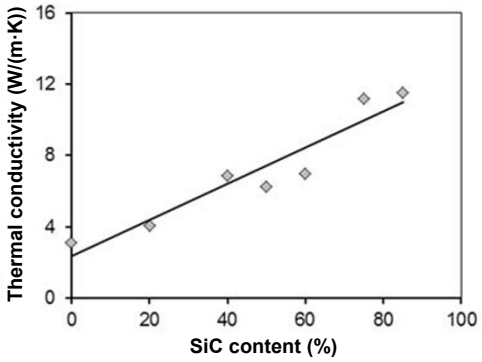

Fig. 13 Effect of SiC content on thermal conductivity coefficient.

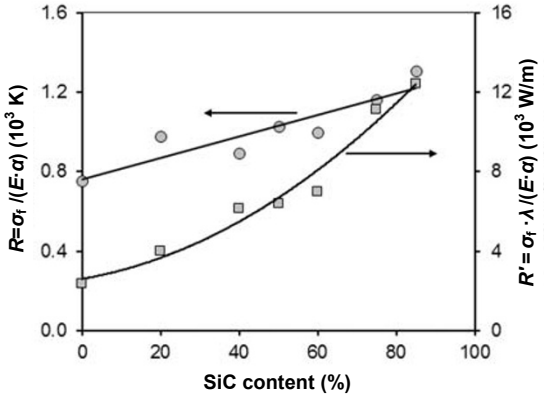

Fig. 14 Effect of SiC content on statistical parameters R and R'.

3.4 Ceramic foam manufacture

Samples of open-cell ceramic foam that can be used as the catalyst support were manufactured from SiC–porcelain ceramics by the polyurethane foam replication process. Details of the process applied in this study are described in Ref. [20]. In brief, reticulated polyurethane foam samples with the nominal cell density of 30 ppi were subjected to multiple impregnation with aqueous suspensions comprising SiC powder and industrial porcelain at the solid residue ratio of 85/15, and carboxymethyl cellulose as the rheological additive (0.1 wt%). After each impregnation using suspensions with the controlled moisture content [20], the samples were subjected to centrifuging to remove excess suspension and drying at 110 ℃. When the targeted porosity of 83%–85% was attained, the samples were sintered in air at 1200 ℃ for 1 h. No visible surface flaw on the foam strut surfaces is observed. Porcelain contains clay and bentonite, which is essential for the sample green density after the start of the polyurethane decomposition. Pore structure of the SiC–porcelain foam synthesized in this study is shown in Fig. 15. Thermal and mechanical properties of the foam were

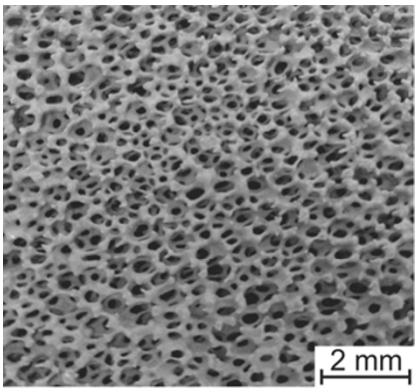

Fig. 15 Pore structure of the SiC–porcelain ceramic foam.

not studied in this research, but they can be estimated from the experimental data on SiC–porcelain ceramic properties using the extensively recognized Ashby's equations [30].

4 Conclusions

Mechanical and thermal properties of SiC–porcelain ceramics were studied in the wide SiC content range of 0–95%. Microstructure evolution, shrinkage at sintering, porosity, mechanical strength, elastic modulus, CTE and thermal conductivity were studied depending on SiC content. The optimal sintering temperature was 1200 ℃, and the maximum three-point bending strength (77 MPa) corresponded to SiC content of 90%. This strength was attained at rather low linear shrinkage at sintering of ~1%. Introducing SiC resulted in the residual porosity increase, including formation of secondary pores due to SiC oxidation and gaseous carbon oxide generation. Higher residual porosity resulted in the more intensive SiC oxidation during the sintering; up to 9% of the introduced SiC oxidized during the sintering. Compared to porcelain ceramics, CTE of this composite ceramics decreased from 5.6×10^{-6} K^{-1} to 5×10^{-6} K^{-1}, and its thermal conductivity increased from 3 W/(m·K) to 12 W/(m·K). Parametric evaluation of the ceramic thermal shock resistance revealed its great potential as the material for thermal cycling applications: higher values of statistical parameters compared to the most conventional engineering ceramics were stated. It was demonstrated that the open-cell foam catalyst supports can be manufactured from SiC–porcelain ceramics by polyurethane foam replication process.

Acknowledgements

The research was supported by Integrated Project T12CO-020 of the National Academy of Sciences of Belarus and Siberian Branch of the Russian Academy of Sciences.

References

[1] Li Y, Wang Y, Zhang Z, *et al.* Oxidative reformings of methane to syngas with steam and CO_2 catalyzed by metallic Ni based monolithic catalysts. *Catal Commun* 2008, **9**: 1040–1044.

[2] Visconti CG, Tronconi E, Groppi G, *et al.* Monolithic catalysts with high thermal conductivity for the Fischer–Tropsch synthesis in tubular reactors. *Chem Eng J* 2011, **171**: 1294–1307.

[3] Sadykov V, Sobyanin V, Mezentseva N, *et al.* Transformation of CH_4 and liquid fuels into syngas on monolithic catalysts. *Fuel* 2010, **89**: 1230–1240.

[4] Smorygo O, Mikutski V, Marukovich A, *et al.* Structured catalyst supports and catalysts for the methane indirect internal steam reforming in the intermediate temperature SOFC. *Int J Hydrogen Energ* 2009, **34**: 9505–9514.

[5] Faure R, Rossignol F, Chartier T, *et al.* Alumina foam catalyst supports for industrial steam reforming processes. *J Eur Ceram Soc* 2011, **31**: 303–312.

[6] Rennard D, French R, Czernik S, *et al.* Production of synthesis gas by partial oxidation and steam reforming of biomass pyrolysis oils. *Int J Hydrogen Energ* 2010, **35**: 4048–4059.

[7] Manfro RL, Ribeiro NFP, Souza MMVM. Production of hydrogen from steam reforming of glycerol using nickel catalysts supported on Al_2O_3, CeO_2 and ZrO_2. *Catalysis for Sustainable Energy* 2013, **1**: 60–70.

[8] Wang C, Wang T, Ma L, *et al.* Steam reforming of biomass raw fuel gas over NiO–MgO solid solution cordierite monolith catalyst. *Energ Convers Manage* 2010, **51**: 446–451.

[9] Twigg MV, Richardson JT. Fundamentals and applications of structured ceramic foam catalysts. *Ind Eng Chem Res* 2007, **46**: 4166–4177.

[10] Lacroix M, Dreibine L, de Tymowski B, *et al.* Silicon carbide foam composite containing cobalt as a highly selective and re-usable Fischer–Tropsch synthesis catalyst. *Appl Catal A*: *Gen* 2011, **397**: 62–72.

[11] Guo X, Cai X, Zhu L, *et al.* Preparation and properties of SiC honeycomb ceramics by pressureless sintering technology. *J Adv Ceram* 2014, **3**: 83–88.

[12] Magnani G, Minoccari GL, Pilotti L. Flexural strength and toughness of liquid phase sintered silicon carbide. *Ceram Int* 2000, **26**: 495–500.

[13] Chen F, Yang Y, Shen Q, *et al.* Macro/micro structure dependence of mechanical strength of low temperature sintered silicon carbide ceramic foams. *Ceram Int* 2012, **38**: 5223–5229.

[14] Soy U, Demir A, Caliskan F. Effect of bentonite addition on fabrication of reticulated porous SiC ceramics for liquid metal infiltration. *Ceram Int* 2011, **37**: 15–19.

[15] Medri V, Fabbri S, Ruffini A, *et al.* SiC-based refractory paints prepared with alkali aluminosilicate binders. *J Eur Ceram Soc* 2011, **31**: 2155–2165.

[16] Medri V, Ruffini A. Alkali-bonded SiC based foams. *J Eur Ceram Soc* 2012, **32**: 1907–1913.

[17] Pan Y, Baptista JL. Low-temperature sintering of silicon carbide with Li_2O–Al_2O_3–SiO_2 melts as sintering aids. *J Eur Ceram Soc* 1996, **16**: 745–752.

[18] Tucker MC, Tu J. Ceramic coatings and glass additives for improved SiC-based filters for molten iron filtration. *Int J Appl Ceram Tec* 2014, **11**: 118–124.

[19] Yao X, Tan S, Zhang X, *et al.* Low-temperature sintering of SiC reticulated porous ceramics with MgO–Al_2O_3–SiO_2 additives as sintering aids. *J Mater Sci* 2007, **42**: 4960–4966.

[20] Leonov AN, Smorygo OL, Sheleg VK. Monolithic catalyst supports with foam structure. *React Kinet Catal L* 1997, **60**: 259–267.

[21] Shui A, Xi X, Wang Y, *et al*. Effect of silicon carbide additive on microstructure and properties of porcelain ceramics. *Ceram Int* 2011, **37**: 1557–1562.

[22] García-Ten J, Saburit A, Bernardo E, *et al.* Development of lightweight porcelain stoneware tiles using foaming agents. *J Eur Ceram Soc* 2012, **32**: 745–752.

[23] Bernardin AM, da Silva MJ, Riella HG. Characterization of cellular ceramics made by porcelain tile residues. *Mat Sci Eng A* 2006, **437**: 222–225.

[24] Smorygo O, Mikutski V, Marukovich A, *et al.* An inverted spherical model of open-cell foam structure. *Acta Mater* 2011, **59**: 2669–2678.

[25] Ritchie RO. Mechanisms of fatigue crack propagation in metals, ceramics and composites: Role of crack tip shielding. *Mat Sci Eng A* 1988, **103**: 15–28.

[26] Kayal N, Dey A, Chakrabarti O. Synthesis of mullite bonded porous SiC ceramics by a liquid precursor infiltration method: Effect of sintering temperature on material and mechanical properties. *Mat Sci Eng A* 2012, **556**: 789–795.

[27] Riedel R, Passing G, Schönfelder H, *et al*. Synthesis of dense silicon-based ceramics at low temperatures. *Nature* 1992, **355**: 714–717.

[28] Gunyaev GM. Polycomponent high-modulus composites. *Polymer Mechanics* 1977, **13**: 685–692.

[29] Lu TJ, Fleck NA. The thermal shock resistance of solids. *Acta Mater* 1998, **46**: 4755–4768.

[30] Ashby MF. The properties of foams and lattices. *Phil Trans R Soc A* 2006, **364**: 15–30.